J Solid State Electrochem (2013) 17:3185–3190
DOI 10.1007/s10008-013-2223-z

ORIGINAL PAPER

Thermodynamics of oxygen in $CaMnO_{3-\delta}$

Ekaterina I. Goldyreva · Ilya A. Leonidov · Mikhail V. Patrakeev · Victor L. Kozhevnikov

Received: 20 June 2013 / Revised: 7 August 2013 / Accepted: 9 August 2013 / Published online: 27 August 2013

Abstract The experimental data for equilibrium oxygen content were used in order to extract increments of partial molar thermodynamic functions of oxygen with changes of oxygen stoichiometry in calcium manganite $CaMnO_{3-\delta}$. It is shown that along with the oxygen exchange reaction, thermal excitation of Mn^{4+} cations plays an important role in equilibration of charged manganese species that appear in response to the loss of oxygen at heating. The interrelation of partial molar enthalpy and entropy of oxygen with electron and ion defect formation parameters is obtained in approximation of the point defect model. The nearly linear changes of oxygen partial molar enthalpy are shown to directly reflect thermally driven changes in concentration of Mn^{3+} cations.

Keywords Calcium manganite · Perovskite-type oxide · Oxygen non-stoichiometry · Partial molar thermodynamic functions

Introduction

High values of electric conductivity, large thermopower and pronounced activity in oxidation reactions attract attention to perovskite-like manganites as materials of importance for use in fuel cells, thermoelectric devices and catalysis [1–6]. The electron transport-related properties of the manganites are associated with the simultaneous presence in their structure of manganese cations in different charged states that appear in response to heterovalent doping and oxygen loss. One of the powerful tools to understand the ensuing defect structure in the manganites is the analysis of the plots of oxygen non-stoichiometry δ vs. oxygen partial pressure p_{O_2} at different temperatures T, the so-called p_{O_2} –T–δ diagrams [7–14]. For instance, it is shown that the equilibrium of manganese species in $La_{1-x}A_xMnO_{3-\delta}$ at $x \leq 0.5$ depends strongly on charge disproportionation reaction $2Mn^{3+}=Mn^{2+}+Mn^{4+}$ [10, 11, 13, 14].

The average oxidation state of manganese increases with doping and approaches 4+ at $x=1$ when oxygen pressure is sufficiently high. At near atmospheric or lower pressures, alkali-earth manganites are oxygen deficient, and it is widely accepted that electrical neutrality of the crystalline lattice in, e.g., $CaMnO_{3-\delta}$, is entirely maintained due to partial reduction of manganese cations, $Mn^{4+} \rightarrow Mn^{3+}$ [15]. The respective p_{O_2} –T–δ diagram for $CaMnO_{3-\delta}$ was obtained in [16]. The authors used experimental isotherms $(3-\delta)$ vs. log p_{O_2} for calculations of partial molar enthalpy $\Delta\overline{H}_O$ and entropy $\Delta\overline{S}_O$ of oxygen in $CaMnO_{3-\delta}$ at temperatures within 950–1050 °C where the cubic structure is stable. More recently [17], we carried out measurements of the p_{O_2} –T–δ diagram at lower temperatures 700–950 °C where all three known high-temperature modifications (orthorhombic, tetragonal and cubic) of $CaMnO_{3-\delta}$ can exist. The attempts proved unsuccessful to simulate the diagram based on the traditional assumption that only a reaction of oxygen exchange

$$2Mn^{3+} + V_O + \frac{1}{2}O_2 = 2Mn^{4+} + O^{2-} \quad (1)$$

takes part in equilibration of manganese species in oxygen-deficient $CaMnO_{3-\delta}$. On the contrary, a rather satisfactory description of the observed experimental data for oxygen

Electronic supplementary material The online version of this article (doi:10.1007/s10008-013-2223-z) contains supplementary material, which is available to authorized users.

E. I. Goldyreva · I. A. Leonidov · M. V. Patrakeev · V. L. Kozhevnikov
Institute of Solid State Chemistry, Ural Branch of Russian Academy of Sciences, 620990 Ekaterinburg, Russian Federation

I. A. Leonidov (✉)
Ural Federal University, 620002 Ekaterinburg, Russian Federation
e-mail: leonidov@imp.uran.ru

non-stoichiometry variation with oxygen pressure and temperature can be achieved when the concomitant reaction

$$2Mn^{4+} = Mn^{3+} + Mn^{5+} \quad (2)$$

is taken into account [18]. This reaction gives rise to some amount of Mn^{5+} cations in $CaMnO_{3-\delta}$ that depends on the ambient atmosphere. It follows from the respective analysis of the p_{O_2} –T–δ diagram that the enthalpy and the entropy for defect formation reactions (1) and (2) in $CaMnO_{3-\delta}$ both depend on the crystalline structure. In particular, the calculated entropy for reaction (1) in the cubic phase occurs in good coincidence with the observed oxidation entropy of $CaMnO_{2.5}$ to $CaMnO_3$ at 950 °C [19]. Additional confirmation to the viability of the defect model involving reactions (1) and (2) follows from a very good correspondence of the enthalpy for reaction (2) and the band gap E_g obtained from DFT calculations of electron band structure in $CaMnO_{3-\delta}$ [20]. It is worth noticing here that reaction (2) of "charge disproportionation" reflects, in fact, thermal excitation of Mn^{4+} cations and formation of t_{2g} holes (Mn^{5+}) and e_g electrons (Mn^{3+}).

Thermodynamic functions of oxygen, $\Delta\overline{H}_O$ and $\Delta\overline{S}_O$, are known to be very sensitive to changes of oxygen content in the structure and, therefore, can provide rather detailed information on defect equilibria in non-stoichiometric oxides [21–24]. Hence, the present work was aimed at calculation of partial molar thermodynamic functions of oxygen in $CaMnO_{3-\delta}$ from the earlier obtained experimental data [17] with the use of defect formation reactions (1) and (2). The relation of the thermodynamic functions of oxygen with defect formation parameters is found, and it is shown that changes in $\Delta\overline{H}_O$ and $\Delta\overline{S}_O$ directly reflect development of reaction (2) at heating.

Results and discussion

Partial molar enthalpy and entropy of oxygen

The chemical potential of oxygen $\Delta\mu_O(\delta,T)$ in $CaMnO_{3-\delta}$ relative to the standard state can be calculated from the pressure-dependent isotherms δ [17] as

$$\Delta\mu_O(\delta,T) \equiv \mu_O\left(CaMnO_{3-\delta}\right) - 1/2\mu_O^o = 1/2RT\cdot \ln p_{O2} \quad (3)$$

where $\mu_{O_2}^o$ is the chemical potential of molecular oxygen in the gas phase at 1 atm, and R is the gas constant. The tetragonal phase is known to occupy a relatively small region in the p_{O_2} –T–δ phase diagram between the low-temperature orthorhombic and high-temperature cubic phases [15]. Consequently, the available experimental data for the tetragonal structure are quite scarce [17]. Therefore, further analysis is limited by the orthorhombic and cubic phases.

The treatment of the experimental data has shown that the plots $\Delta\mu_O(\delta,T)$ at permanent δ depend linearly on temperature both in orthorhombic and cubic modifications of $CaMnO_{3-\delta}$, Fig. 1. Hence, the partial molar enthalpy $\Delta\overline{H}_O$ and entropy $\Delta\overline{S}_O$ of oxygen can be obtained from the known thermodynamic interrelation

$$\Delta\mu_O(\delta,T) = \Delta\overline{H}_O - T\Delta\overline{S}_O \quad (4)$$

It is seen from the respective plots in Figs. 2 and 3 that the temperature variations of thermodynamic functions in $CaMnO_{3-\delta}$ lie practically within experimental errors. At the same time, the transformation of the crystalline structure is accompanied with considerable changes in $\Delta\overline{H}_O$ and $\Delta\overline{S}_O$. This difference is quite expected because $\Delta\overline{H}_O$ and $\Delta\overline{S}_O$ both depend on enthalpy $\Delta H°$ and entropy $\Delta S°$ of the defect formation reactions [21, 25]. Therefore, the absolute values of

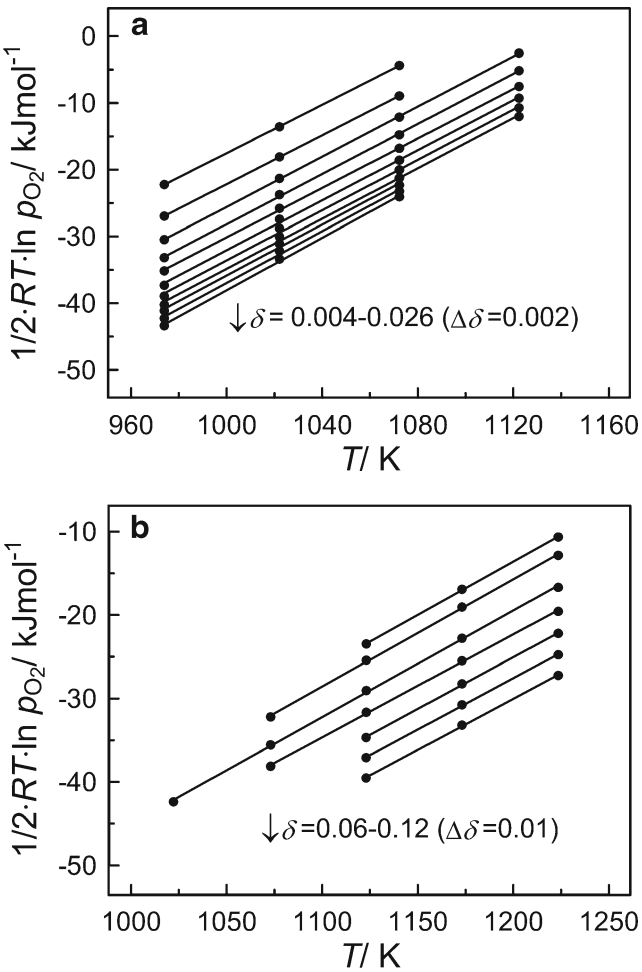

Fig. 1 Plots of $^1/_2RT\cdot\ln p_{O_2}$ vs. temperature at different δ in $CaMnO_{3-\delta}$ with orthorhombic (**a**) and cubic (**b**) structure

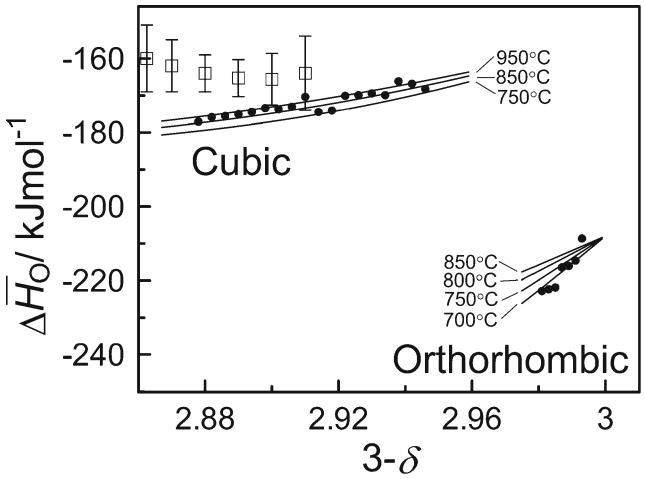

Fig. 2 Plots of partial molar enthalpy $\Delta\overline{H}_O$ vs. oxygen content $(3-\delta)$ in orthorhombic and cubic $CaMnO_{3-\delta}$. *Dots* show experimental values (uncertainty ±3 kJ mol^{-1}); *solid lines* show results of calculations with the help of Eq. (21) at T= const. The *empty squares* show data [16]

$\Delta\overline{H}_O$ and $\Delta\overline{S}_O$, larger in the orthorhombic than in the cubic phase, can be interpreted as reflecting respective differences of $\Delta H°$ and $\Delta S°$ in the structural modifications of $CaMnO_{3-\delta}$ (Table 1) [18]. One can add also that $\Delta\overline{H}_O$ and $\Delta\overline{S}_O$, obtained in the present work for the cubic phase, are in excellent correspondence with the respective data [16].

Thermodynamic model for $CaMnO_{3-\delta}$

The free Gibbs energy, G, for $CaMn_n^{3+}Mn_g^{4+}Mn_p^{5+}O_{3-\delta}$ can be expressed as

$$G = G^\circ + \mu^\circ(Ca^{2+}) + n\mu^\circ(Mn^{3+}) + g\mu^\circ(Mn^{4+}) + p\mu^\circ(Mn^{5+}) + (3-\delta)\mu^\circ(O^{2-}) + \delta\mu^\circ(V_O) + TS(\text{conf}) \quad (5)$$

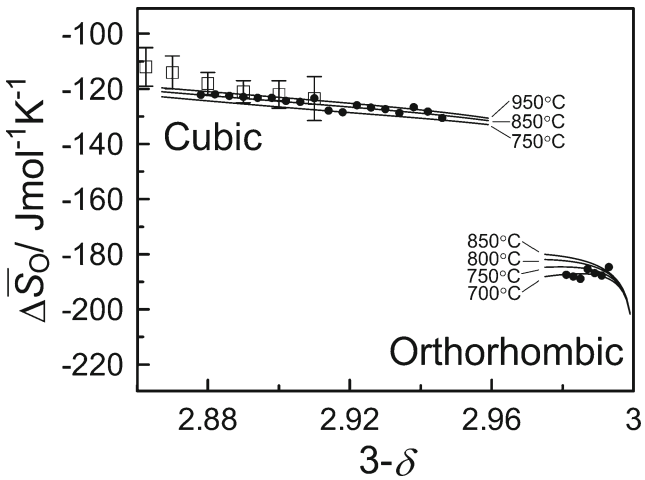

Fig. 3 Plots of partial molar entropy $\Delta\overline{S}_O$ vs. oxygen content $(3-\delta)$ in orthorhombic and cubic $CaMnO_{3-\delta}$. *Dots* show experimental values (uncertainty ±2 J mol^{-1} K^{-1}); *solid lines* show results of calculations with the help of Eq. (22) at T= const. The *empty squares* show data [16]

where symbols $\mu°$ designate δ independent parts of chemical potentials of respective defects. Following [21], we assume that interaction energies between the species entering reactions (1) and (2) are included in $\mu°$. The configuration entropy $S(\text{conf})$ can be calculated as

$$S(\text{conf}) = k\left[\ln\frac{N!}{(Nn)!(Ng)!(Np)!} + \ln\frac{(3N)!}{(N(3-\delta))!(N\delta)!}\right] \quad (6)$$

where k is Boltzmann's constant and N is Avogadro's number. The chemical potential μ_O of oxygen in $CaMnO_{3-\delta}$ can be obtained by partial differentiation of Eq. (5)

$$\mu_O = \frac{\partial G}{\partial(3-\delta)} = -\frac{\partial G}{\partial\delta} = -\frac{\partial n}{\partial\delta}\mu^\circ(Mn^{3+}) - \frac{\partial g}{\partial\delta}\mu^\circ(Mn^{4+}) - \frac{\partial p}{\partial\delta}\mu^\circ(Mn^{5+}) + \mu^\circ(O^{2-}) - \mu^\circ(V_O) - Ts_O(\text{conf}) \quad (7)$$

where

$$s_O(\text{conf}) = -\frac{\partial S(\text{conf})}{\partial\delta} \quad (8)$$

The application of Stirling's formula to Eq. (8) results in

$$s_O(\text{conf}) = R\left[\frac{\partial n}{\partial\delta}(\ln n + 1) + \frac{\partial g}{\partial\delta}(\ln g + 1) + \frac{\partial p}{\partial\delta}(\ln p + 1)\right] + R\ln\frac{\delta}{3-\delta} \quad (9)$$

where $R = N\cdot k$ is the gas constant. Combining the electrical neutrality

$$n = p + 2\delta \quad (10)$$

and the site conservation

$$g + n + p = 1 \quad (11)$$

requirements with the equilibrium constant for reaction (2)

$$K_D = \frac{[Mn^{3+}][Mn^{5+}]}{[Mn^{4+}]^2} = n\cdot p/g^2 \quad (12)$$

Table 1 The enthalpy and entropy for reactions (1) and (2) in orthorhombic and cubic $CaMnO_{3-\delta}$ [18]

Structure	ΔH°_{Ox}, kJ mol^{-1}	ΔS°_{Ox}, kJ mol^{-1} K^{-1}		ΔH°_{D}, kJ mol^{-1}	ΔS°_{D}, kJ mol^{-1} K^{-1}	E_g, kJ mol^{-1}
Orthorhombic	−286±10	−177±8		78.0±4.0	42.4±2.2	67.5 [20]
Cubic	−190±7	−92±5	−95 [19]	33.4±1.8	−3.0±0.4	44.4 [20]

yields

$$\frac{\partial n}{\partial \delta}=\frac{\partial p}{\partial \delta}+2;\quad \frac{\partial g}{\partial \delta}+\frac{\partial n}{\partial \delta}+\frac{\partial p}{\partial \delta}=0;\qquad \frac{\partial n}{\partial \delta}=1+\frac{2\delta}{4K_D\cdot g+n+p} \tag{13}$$

Then, the chemical potential of oxygen in $CaMnO_{3-\delta}$ follows from Eqs. (7) and (9) as

$$\mu_O=2\mu^{\circ}(Mn^{5+})-2\mu^{\circ}(Mn^{4+})+\frac{\partial n}{\partial \delta}\left[2\mu^{\circ}(Mn^{4+})-\mu^{\circ}(Mn^{3+})-\mu^{\circ}(Mn^{5+})\right]+\mu^{\circ}(O^{2-})-\mu^{\circ}(V_O)-Ts_O(\text{conf}) \tag{14}$$

where s_O(conf) is expressed as

$$s_O(\text{conf})=R\left(\ln\frac{\delta\cdot g^2}{(3-\delta)\cdot p^2}+\frac{\partial n}{\partial \delta}\ln K_D\right) \tag{15}$$

Defect formation parameters and partial molar thermodynamic functions of oxygen

The changes of free Gibbs energy for reactions (1) and (2) are related with the chemical potentials of ions and defects

$$\Delta G^{\circ}_{Ox}=\mu^{\circ}(O^{2-})-\mu^{\circ}(V_O)+2\left[\mu^{\circ}(Mn^{4+})-\mu^{\circ}(Mn^{3+})\right]-\frac{1}{2}\mu^{\circ}(O_2) \tag{16}$$

and

$$\Delta G^{\circ}_{D}=\mu^{\circ}(Mn^{3+})+\mu^{\circ}(Mn^{5+})-2\mu^{\circ}(Mn^{4+}) \tag{17}$$

Since

$$2\mu^{\circ}_O=\mu^{\circ}_{O_2} \tag{18}$$

the joint use of Eqs. (14) and (16)–(18) results in

$$\Delta\mu_O=\mu_O-\mu^{\circ}_O=\Delta G^{\circ}_{Ox}+2\Delta G^{\circ}_{D}-\frac{\partial n}{\partial \delta}\Delta G^{\circ}_{D}-Ts_O(\text{conf}) \tag{19}$$

Recalling that the change of the free Gibbs energy ΔG°_j is related with the changes of standard enthalpy, ΔH°_j, and entropy, ΔS°_j, for respective reactions as

$$\Delta G^{\circ}_j=\Delta H^{\circ}_j-T\Delta S^{\circ}_j \tag{20}$$

one can obtain the enthalpy and entropy contributions to Eq. (19) as

$$\Delta\overline{H}_O=\Delta H^{\circ}_{Ox}+2\Delta H^{\circ}_{D}-\frac{\partial n}{\partial \delta}\Delta H^{\circ}_{D} \tag{21}$$

$$\Delta\overline{S}_O=\Delta S^{\circ}_{Ox}+2\Delta S^{\circ}_{D}-\frac{\partial n}{\partial \delta}\Delta S^{\circ}_{D}+s_O(\text{conf}) \tag{22}$$

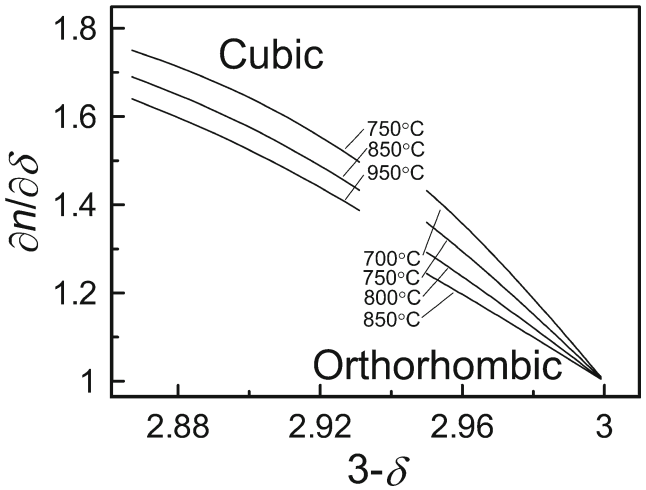

Fig. 4 Isothermal plots of $\partial n/\partial\delta$ vs. oxygen content $(3-\delta)$ in orthorhombic and cubic $CaMnO_{3-\delta}$ as calculated with the help of Eq. (13)

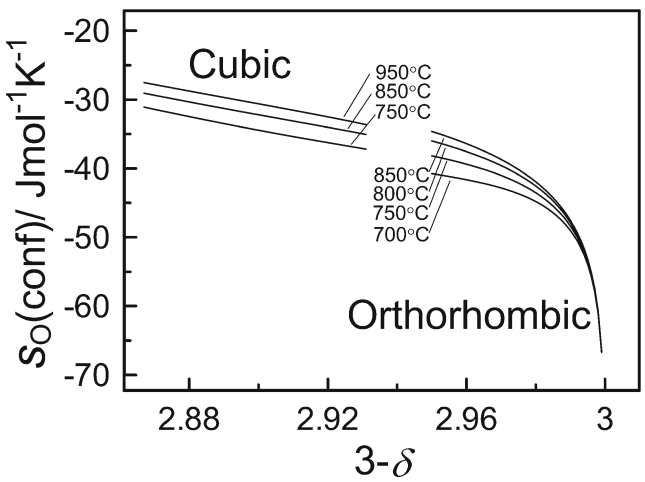

Fig. 5 Isothermal plots of s_O(conf) vs. oxygen content $(3-\delta)$ in orthorhombic and cubic $CaMnO_{3-\delta}$ as calculated with the help of Eq. (15)

Relations (21) and (22) can be employed in order to calculate changes in the molar thermodynamic functions with non-stoichiometry.

Calculation of partial molar thermodynamic functions

The values of ΔH°_{Ox}, ΔS°_{Ox} and ΔH°_{D}, ΔS°_{D} in Table 1 are used for calculations of $\Delta\overline{H}_O$ and $\Delta\overline{S}_O$. The concentration values n, g and p for differently charged manganese species Mn^{3+}, Mn^{4+} and Mn^{5+}, respectively, and oxygen non-stoichiometry in $CaMn_n^{3+}Mn_g^{4+}Mn_p^{5+}O_{3-\delta}$ are found from Eqs. (10)–(12) as

$$p = \frac{\delta + 2K_D - 4\delta K_D - D}{4K_D - 1}, \quad n = p + 2\delta, \quad g = 1 - n - p \quad (23)$$

Here, $D = \sqrt{K_D - 4\delta^2 K_D + \delta^2}$, and K_D is the equilibrium constant for reaction (2), which depends on temperatures as

$$K_D = \exp\left(\Delta S^{\circ}_D / R\right)\exp\left(-\Delta H^{\circ}_D / RT\right) \quad (24)$$

The obtained isothermal plots for $\partial n/\partial\delta$ exhibit a noticeable decrease with δ in both orthorhombic and cubic phases (Fig. 4). The using of this result in Eq. (21) may help in the understanding of the origin of approximately a linear increase of $\Delta\overline{H}_O$ with oxygen content in $CaMnO_{3-\delta}$ (Fig. 2). The calculated results for configuration entropy, Eq. (15), are shown in Fig. 5. The variations of s_O(conf) are relatively small in the cubic phase. At the same, the configuration entropy is seen to progressively decrease in the orthorhombic phase at $\delta \to 0$. The partial molar enthalpy $\Delta\overline{H}_O$ and entropy $\Delta\overline{S}_O$ of oxygen in $CaMnO_{3-\delta}$ can be calculated from Eqs. (21) and (22) with the help of the obtained $\partial n/\partial\delta$ and s_O(conf). Respective results in Figs. 2 and 3 show a good coincidence of the calculated and experimental data in both crystalline modifications.

According to Eqs. (13) and (15), the concentration of manganese species n, g, and p, and oxygen deficiency δ, depend on temperature which, in turn, results in a weak temperature dependence of calculated values for $\Delta\overline{H}_O$ and $\Delta\overline{S}_O$. These small temperature variations lie within experimental uncertainties so that experimental values in Figs. 2 and 3 can be considered as average over studied limits of temperature. The stronger δ dependence of $\Delta\overline{H}_O$ in the orthorhombic than in the cubic phase (Fig. 2) is indicative of respectively faster variations of $\partial n/\partial\delta$ in the orthorhombic structural modification of $CaMnO_{3-\delta}$.

Conclusions

The chemical potential of oxygen in $CaMnO_{3-\delta}$ relative to the standard state is calculated from the experimental p_{O_2} –T–δ diagram. The partial molar enthalpy $\Delta\overline{H}_O$ and entropy $\Delta\overline{S}_O$ of oxygen is obtained from the linear plots of $\Delta\mu_O(\delta,T)$ vs. temperature. The partial thermodynamic functions of oxygen in $CaMnO_{3-\delta}$ are found to depend on non-stoichiometry and crystalline structure. The interrelation of partial molar thermodynamic functions of oxygen with defect formation parameters is found based on thermodynamic analysis of defect equilibrium in $CaMnO_{3-\delta}$. The good coincidence of experimental and calculated values for partial molar thermodynamic functions demonstrates applicability of the ideal solution approximation for description of electron defects and oxygen vacancies in $CaMnO_{3-\delta}$. It is found that the concentration of Mn^{3+} cations significantly depends on solid–gas phase oxygen exchange and intrinsic reaction of thermal excitation of Mn^{4+} cations. As a result, the partial molar enthalpy and entropy of oxygen in $CaMnO_{3-\delta}$ both occur to strongly depend on non-stoichiometry.

Acknowledgments The authors gratefully acknowledge partial support of this work by the Russian Foundation for Basic Research (grant no. 12-03-31217) and the Presidium of Ural Branch of RAS (grant no. 12-M-23-2061).

References

1. Adler SB (2004) Chem Rev 104:4791
2. Tsipis EV, Kharton VV (2008) J Solid State Electrochem 12:1367–1391
3. Radhakrisnan R, Virkar AV, Singhal SC (2005) J Electrochem Soc 152:A210–A218
4. Werchmeister RML, Hansen KK, Mogensen M (2010) Mater Res Bull 45:1554–1561
5. Ohtaki M, Koga H, Tokunaga T, Eguchi K, Arai H (1995) J Solid State Chem 105:105–111
6. Wang Y, Sui Y, Wang X, Su W (2009) J Phys D Appl Phys 42:055010
7. Kamata K, Nakajima T, Hayiashi T, Nakamura T (1978) Mater Res Bull 13:49–54
8. Nakamura T, Petzow G, LG G (1979) Mater Res Bull 14:649–659
9. Kamegashira N, Miyazaki Y, Yamamoto H (1984) Mater Chem Phys 11:187–194
10. Kuo JH, Anderson HU, Sparlin DM (1989) J Solid State Chem 83:52–60
11. Van Roosmalen JAM, Corfunke EHP (1994) J Solid State Chem 110:109–112
12. Van Roosmalen JAM, Corfunke EHP (1994) J Solid State Chem 110:113–117
13. Mizusaki J, Tagava H, Naraya K, Sasamoto T (1991) Solid State Ionics 49:111–118
14. Mizusaki J, Mori N, Takai H, Yonemura Y, Minamiue H, Tagava H, Dokiya M, Inaba H, Naraya K, Sasamoto T, Hashimoto T (2000) Solid State Ionics 129:163–177

15. Rørmark L, Wiik K, Stølen S, Grande T (2002) J Mater Chem 12:1058–1067
16. Bakken E, Norby T, Stølen S (2005) Solid State Ionics 176:217–223
17. Leonidova EI, Leonidov IA, Patrakeev MV, Kozhevnikov VL (2011) J Solid State Electrochem 15:1071–1075
18. Goldyreva EI, Leonidov IA, Patrakeev MV, Kozhevnikov VL (2012) J Solid State Electrochem 16:1187–1191
19. Bakken E, Boerio-Goates J, Grande T, Hovde B, Norby T, Rørmark L, Stevens R, Stølen S (2005) Solid State Ionics 176:2261–2267
20. Søndenå R, Stølen S, Ravindran P, Grande T, Grande NL (2007) Phys Rev B 75:184105
21. Mizusaki J, Yoshishiro M, Yamauchi S, Fueki K (1987) J Solid State Chem 67:1–8
22. Park CY, Jacobson AJ (2005) J Electrochem Soc 152:J65–J73
23. Søgaard M, Hendriksen PV, Mogensen M (2007) J Solid State Chem 180:1489–1503
24. Yoo J, Jacobson AJ (2009) J Electrochem Soc 156:B1085–B1091
25. Kofstad P (1972) Nonstoichiometry, diffusion and electrical conductivity in binary metal oxides. Wiley-Interscience, New York